Received: 24 June 2020 | Revised: 14 August 2020 | Accepted: 18 September 2020

DOI: 10.1111/joa.13332

ORIGINAL PAPER

ANATOMICAL SOCIETY Journal of Anatomy WILEY

Histological and molecular characterization of the growing nasal septum in mice

Pranidhi Baddam[1] | Tiffany Kung[1] | Adetola B. Adesida[2] | Daniel Graf[1,3]

[1]School of Dentistry, Faculty of Medicine and Dentistry, University of Alberta, Edmonton, AB, Canada

[2]Department of Surgery, Faculty of Medicine and Dentistry, University of Alberta, Edmonton, AB, Canada

[3]Department of Medical Genetics, Faculty of Medicine and Dentistry, University of Alberta, Edmonton, AB, Canada

Correspondence
Daniel Graf, Faculty of Medicine and Dentistry, School of Dentistry, University of Alberta, 7020N Katz Group Centre for Pharmacy & Health Research, 11361-87 Avenue, Edmonton, AB, Canada T6G 2E1.
Email: dgraf@ualberta.ca

Funding information
Natural Sciences and Engineering Research Council of Canada, Grant/Award Number: RGPIN-2014-06311; University of Alberta

Abstract

The nasal septum is a cartilaginous structure that serves as a pacemaker for the development of the midface. The septum is a hyaline cartilage which is surrounded by a perichondrium and epithelium. It remains cartilaginous anteriorly, but posteriorly it undergoes endochondral ossification to form the perpendicular plate of the ethmoid. Understanding of hyaline cartilage differentiation stems predominantly from investigations of growth plate cartilage. It is currently unclear if the morphological and molecular properties of the differentiating nasal septum align with what is known from the growth plate. In this study, we describe growth, molecular, and cellular characteristics of the nasal septum with reference to hyaline cartilage differentiation. The nasal septum grows asynchronous across its length with phases of rapid growth interrupted by more stagnant growth. Growth appears to be driven predominantly by acquisition of chondrocyte hypertrophy. Similarly, cellular differentiation is asynchronous, and differentiation observed in the anterior part precedes posterior differentiation. Overall, the nasal septum is structurally and molecularly heterogeneous. Early and extensive chondrocyte hypertrophy but no ossification is observed in the anterior septum. Onset of hypertrophic chondrocyte differentiation coincided with collagen fiber deposition along the perichondrium. Sox9, Col2, Col10, Mmp13, Sp7, and Runx2 expression was heterogeneous and did not always follow the expected pattern established from chondrocyte differentiation in the growth plate. The presence of hypertrophic chondrocytes expressing bone-related proteins early on in regions where the nasal septum does not ossify displays incongruities with current understanding of hyaline cartilage differentiation. Runx2, Collagen II, Collagen X, and Sp7 commonly used to mark distinct stages of chondrocyte maturation and early bone formation show wider expression than expected and do not align with expected cellular characteristics. Thus, the hyaline cartilage of the nasal septum is quite distinct from growth plate hyaline cartilage, and caution should be taken before assigning cartilage properties to less well-defined cartilage structures using these commonly used markers. Beyond the structural description of the nasal cartilage, this study also provides important information for cartilage tissue engineering when using nasal septal cartilage for tissue regeneration.

KEYWORDS

chondrocyte differentiation markers, extracellular matrix, hyaline cartilage development, mouse, nasal septum

1 | INTRODUCTION

The nasal septum is a cartilaginous structure that divides the nasal cavity and provides structural support to the midface (Kim et al., 2008). The septum is a heterogeneous structure with the anterior part remaining cartilaginous throughout life, whereas parts of the posterior septum undergo endochondral ossification to form the perpendicular plate of ethmoid (PPE; Kim et al., 2008). Structurally, the nasal septum is composed of a dense network of chondrocytes, extracellular matrix (ECM), and flanked by a perichondrium (Harkema, 2015). Whether the septum also serves a mechanical role besides structural support is controversial. It has been proposed that its stiff cartilage properties serve to absorb stresses resulting from midfacial growth and impact forces from mastication (Al Dayeh & Herring, 2014). The stiffness, rigidity, and appearance of the nasal septum cartilage are characteristics of hyaline cartilage.

Hyaline cartilage is the simplest type of cartilage, and due to its relatively uniform structure is also referred to as immature cartilage (Grogan et al., 2009; Varela-Eirin et al., 2018). It is found in different areas in the body, including growth plates of long bones, the knees, as well as the nasal septum. Our detailed molecular and cellular understanding on hyaline cartilage stems predominantly from studies investigating growth plates, articular joints, and pathologies associated with cartilage degeneration such as osteoarthritis of the knee. In the growth plate, hyaline cartilage is temporary and is required to support growth of this initially avascular skeletal structure. It is typically replaced by bone through a process called endochondral ossification. During this process, chondrocytes will either undergo apoptosis to be replaced by bone-forming osteoblasts, transdifferentiate into osteoblasts to form bone themselves, or differentiate into mature, hypertrophic chondrocytes to maintain the cartilage (Cervantes-Diaz et al., 2017). Hyaline cartilage in articular joints serves a very different, primarily load bearing function and will remain cartilaginous throughout life (Marconi et al., 2020).

There is considerable literature on the contribution of the nasal septum for midfacial growth. The nasal septum has been recognized as pacemaker for midfacial development (Hall & Precious, 2013). Its resection interferes with midfacial growth (Moss et al., 1968; Sarnat & Wexler, 1967; Stenström & Thilander, 1970). Children with midfacial hypoplasia often present with nasal septum deviation, although the significance of this malformation is not understood (D'Ascanio et al., 2010; Kemble, 1973; Westreich et al., 2011). Because of its hyaline characteristics, nasal septum cartilage is being explored as source for autologous chondrocytes that can be used for articular cartilage repair (Mumme et al., 2016). A recent a phase I clinical study explored the use of nasal septum cartilage as source to repair cartilage defects in osteoarthritis patients (Mumme et al., 2016). Several studies have described the growth pattern of the nasal septum either in the context of growth anomalies in children/adolescents such as midfacial hypoplasia and nasal septum deviation (Goergen et al., 2017) or in large animals mapping proliferation using a histological approach (Al Dayeh & Herring, 2014; Al Dayeh et al., 2013; Gupta, 2011; Long et al., 1968). A detailed growth analysis at the PPE revealed that nasal septum growth must involve mechanisms other than cell proliferation at the plate itself (Wealthall & Herring, 2006). A systematic study focusing on the development and maturation combining growth, histological, and immunofluorescence analysis of the entire septum has yet to be done. It remains unclear if and how molecular properties of nasal septum chondrocytes change over time, and how they differ from articular chondrocytes. One might expect that the different functional requirements *in vivo* are reflected in differences in cellular and molecular differences.

Gene regulatory networks involving Sox9, Runx2, and Sp7 were identified as core regulators of cartilage and bone differentiation (Gómez-Picos & Eames, 2015). Sox9 is an early, key transcriptional regulator essential for chondrocyte differentiation. It is required for the formation of all cartilages (Bi et al., 1999; Gómez-Picos & Eames, 2015; Kozhemyakina et al., 2015). It is first expressed in the condensing mesenchyme, but can also be found later in mature, hypertrophic chondrocytes co-expressed with Runx2 (Gómez-Picos & Eames, 2015). Immature cartilage is rich in sulfated proteoglycans, and stains strongly with Safranin O and Alcian Blue (Gómez-Picos & Eames, 2015). The ECM of immature cartilage is characterized by high amounts of collagen II (Col2) (Cattell et al., 2011; Gómez-Picos & Eames, 2015). In contrast, mature cartilage contains comparatively fewer proteoglycans resulting in less intense staining with Safranin O and Alcian Blue. Levels of Col2 are decreased, and the presence of collagen X (Col10) is often observed (Robins et al., 2006). The presence of matrix metallopeptidase 13 (Mmp13) is associated with the degradation of Col2 and the invasion of vasculature to support osteoprogenitor cells (Kozhemyakina et al., 2015). Sp7 (Osterix) is a key transcriptional regulator for bone-depositing osteoblasts (Hojo et al., 2016). Osteocalcin (Ocn), secreted by osteoblasts and one of the most abundant components of the bone mineral matrix, is a commonly used marker for bone formation (Zoch et al., 2016). Collagen I (Col1) is the most prevalent collagen in the bone mineral matrix (Cervantes-Diaz et al., 2017; Robins et al., 2006). Many of the markers commonly used for mature cartilage overlap with bone (Gómez-Picos & Eames, 2015). For instance, Sp7 is also expressed in mature cartilage, and Runx2 is not only expressed during endochondral ossification, but also in chondrocyte progenitor cells (Cattell et al., 2011; Enomoto et al., 2004). The ECM of cartilage is very diverse and contains several types of collagen at one time (Robins et al., 2006). Despite this complexity, Col2 and Sox9 are commonly used as markers for immature cartilage, Mmp13, Col10, and Runx2 as markers for hypertrophic chondrocyte, and Col1, Sp7, and Ocn as bone markers in alignment to their expression in the cartilaginous growth zone of long bones. There is increasing realization that classifying cartilages on the basis of expression of those molecular markers is an oversimplification. It does not truly reflect the complexity and molecular requirements for the development of specialized hyaline cartilages in different anatomical locations.

In this study, we investigated the growth and maturation of nasal hyaline cartilage and correlated it with the commonly used molecular properties for growth plate cartilage. Based on previous literature, it was not fully resolved when and where nasal cartilage growth occurs (Vora et al., 2016; Wealthall & Herring, 2006) and how this growth correlates with cellular characteristics described

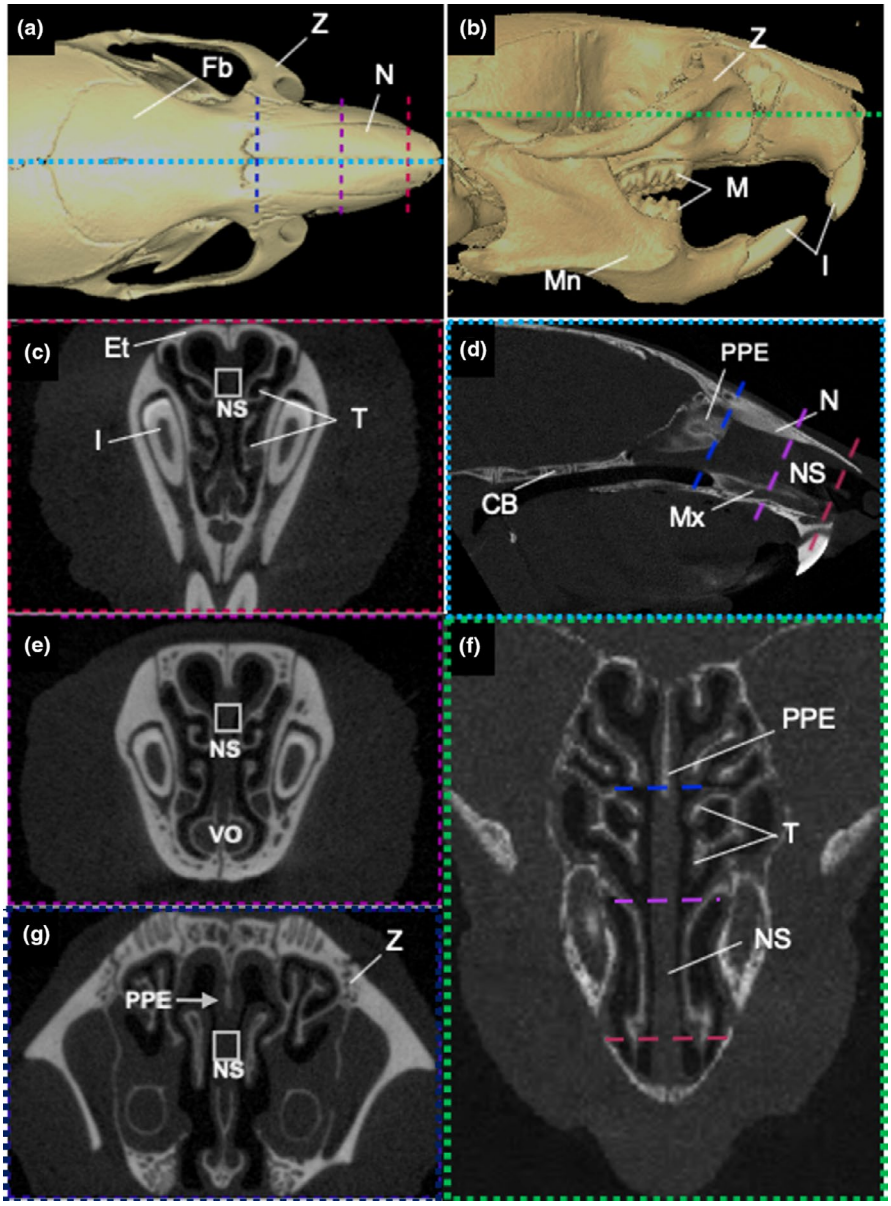

FIGURE 1 μCT representation indicating the position of vertical planes used for μCT and histological analysis. (a,b) Isosurface representation of a μCT scan of an adult mouse indicating (c) anterior (red), (e) a–p midpoint (purple), and (g) posterior (dark blue) regions of the nasal septum. White boxes indicate the corresponding region where histological stains and immunofluorescence used for imaging. (d) Mid-sagittal (light blue) and (f) axial (green) representation of the PPE and NS. μCT, micro-computed tomography; CB, cranial base; Et, ethmoid; Fb, frontal bone; I, incisors; M, molars; Mn, mandible; Mx, maxilla; N, nasal bone; NS, nasal septum; PPE, perpendicular plate of ethmoid; T, turbinates; VO, vomer; Z, zygomatic bone

for maturation of other hyaline cartilages (Gómez-Picos & Eames, 2015; Las Heras et al., 2012). We characterized dynamic changes in the nasal septum cartilage using micro-CT, histological staining, and immunofluorescence at several time-points during development. We find that the nasal septum cartilage is a surprisingly dynamic and complex structure displaying significant anterior-posterior (A-P) differences. It undergoes significant remodeling during and post rapid midfacial growth that contributes to nasal septum growth through the process of chondrocyte hypertrophy.

2 | METHODS

2.1 | Mice

Animal experiments were approved by the Research Ethics office of the University of Alberta (Animal Use and Care Committee protocol AUP1149) in compliance with guidelines by the Canadian Council of Animal Care. C57BL/6J mice were euthanized at embryonic day 18.5 (E18.5), and postnatal (PN) days 0, 7, 14, 21, 30, and 60 for this study. These time-points were chosen to represent different stages in nasal cavity growth development as established by Vora et al. (2016). After euthanasia, mice were perfused and fixed using 4% paraformaldehyde for 24 h prior to further analysis.

2.2 | Micro-computed tomography analysis

Mice heads (n = 3/age) were scanned using MILabs micro-computed tomography (μCT; Milabs) at the School of Dentistry, University of Alberta. The following parameters were applied for scanning: voxel size = 10 μm; voltage = 50 kV; current = 0.24 mA; and exposure time = 75 ms. Scans were reconstructed from 3600 individual projections at a voxel size of 25 μm and analyzed using

AMIRA software (Thermo Scientific). Scans were realigned prior to analysis such that the *xz*-axis corresponds to vertical line of the nasal septum. The anterior nasal septum was defined as the region anterior to the appearance of the ossified vomer. The articulation of the frontal bones with ethmoid was considered as the posterior nasal septum with the midpoint of the anterior and posterior nasal septum (a–p midpoint) describing a medial nasal septum (Figure 1). The set of landmarks described in (Vora et al., 2016) was used to quantify growth of the nasal septum and cavity at anterior, a–p midpoint, and posterior positions or on a midsagittal region, respectively, as demonstrated in Figure 2.

2.3 | Tissue preparation and histology

Mice skulls were decalcified using ethylenediaminetetraacetic acid from 1 day (PN0 heads) to 6 weeks (PN60 heads) before processing for paraffin embedding. Tissues were processed in increasing ethanol gradient washes (75% v/v, 95% v/v, 100%) and xylol prior to being embedding in paraffin. Paraffin blocks were sectioned using a Reichert HistoSTAT rotary microtome. The nasal septum was sectioned at 7 μm in a frontal orientation.

2.4 | Safranin O, Van Gieson, and Alcian Blue staining

Safranin O, Van Gieson, and Alcian Blue staining was performed according to publicly available protocols from IHC World (n.d.). Anterior, a–p midpoint, and posterior nasal septum paraffin sections were stained. Only selected ages (PN0, PN7, PN21, PN30, PN60) are shown, with additional ages (E18.5, PN14) provided in Supporting Information figures. Safranin O and Alcian blue were used to stain cartilage, and Van Gieson was used to identify collagen fibers in the nasal septum.

2.5 | Immunofluorescence

For immunofluorescence staining sections were de-paraffinized in xylol and rehydrated in a decreasing ethanol gradient. Antigens were retrieved by digesting with Hyaluronidase (Sigma-Aldrich H3506) (272 μM) for 30 min on a heat block at 37°C in a humidified chamber. Goat/Donkey serum was used to block the sections and primary antibodies were incubated overnight at 4°C. The details of the primary antibodies are as follows: Col2 (clone 2b1.5, Abcam, ab185430), Sox9

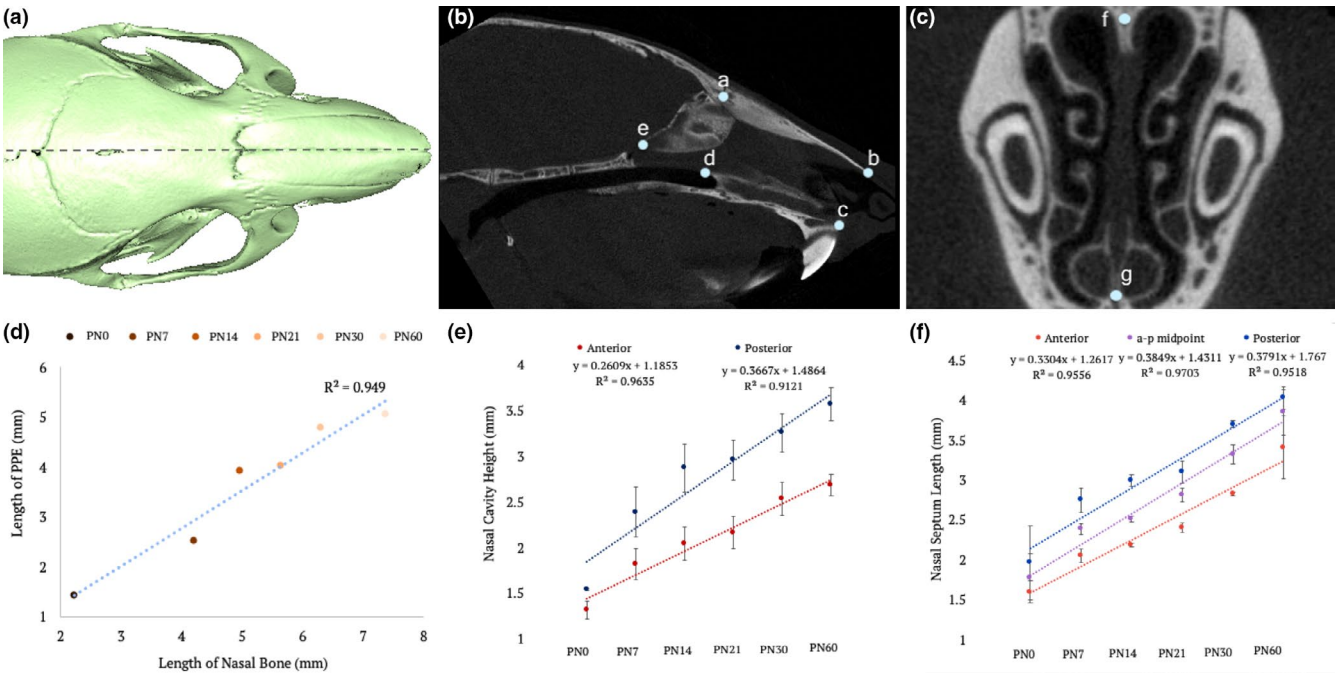

FIGURE 2 Mapping the dynamic growth of the nasal septum. Landmark-based quantitative analysis was conducted on μCT scans of mice ages PN0, 7, 14, 21, 30, and 60 ($n = 3$ for PN0, 7, and 60 and $n = 5$ for PN14, 21, and 30). For growth analysis of the nasal cavity, midsagittal cross-section was used (A) to place the landmarks (B,C). (D) Plotting length of the nasal bone (a,b) against the length of the PPE (a–e) over time demonstrates a linear trend (blue line) indicating concomitant growth of nasal bone and PPE. A growth arrest is evident between PN14 and 21. (E) Height of nasal cavity at anterior (red, landmarks b,c) and posterior (blue, landmark a–d) positions plotted against the different ages. Trendline and slope show overall linear growth with a faster growth rate posterior. A growth arrest is evident between P14 and P21. (F) Septum length (landmarks f,g) at anterior (red), a–p midpoint (purple), and posterior (blue) positions plotted against the different ages. Trendline and slope show overall linear growth with almost comparable growth at all three positions. Note that period of reduced growth occurs at a different time depending on location. Landmarks used are described in Vora et al. (2016). Graphs demonstrate means at each time-point with error bars representing standard deviations when applicable ($n = 3$ for PN0, 7, 60 and $n = 5$ for PN14, 21, 30). Linear trendline, slope, and correlation coefficient (R^2) are expressed for D–F. μCT, micro-computed tomography; PPE, perpendicular plate of ethmoid

(clone EPR14335-78, Abcam, ab185966), Mmp13 (clone C-3, Santa Cruz Biotechnology, sc515284), Runx2 (Novus Biologicals, nbp1-77461), Osterix (Sp7) (Abcam, ab94744), Ocn (Abcam, ab93876), Col10 (clone X-AC9, Santa Cruz Biotechnologies, sc59954), and normal mouse IgG1 (Santa Cruz Biotechnology, sc3877). Secondary antibodies used were donkey anti-rabbit Alexa647 (Life Technologies, a31573) and goat anti-mouse IgG1-Alexa647 and IgG2a-Alexa647 (Thermo Fisher Scientific, a21240, a21241). All sections were counterstained with 4',6-Diamidino-2-Phenylindole (DAPI) (1:1500 dilution of 100 ng/ml stock solution). Slides were imaged using an IXplore Standard Olympus Compound microscope. All staining was done at least three times on different specimens for each antibody and age. Autofluorescence and antibody controls are shown in Figure S4.

2.6 | Data analysis

Graphs indicate mean ± standard deviation when applicable to demonstrate variability between mice within each age group. Additionally, trendlines with slopes and correlation coefficients are added when demonstrating a relationship between two variables over time using Microsoft Excel.

3 | RESULTS

3.1 | The nasal cavity shows dynamic growth phases between birth and adulthood

To understand if and when regional growth differences occur in the nasal septum, a landmark-based (Vora et al., 2016) nasal septum growth analysis of wild-type mice scans at PN0, 7, 14, 21, 30, and 60 was performed. We found that the nasal cavity growth is complex with anterior (Figure 1c), a–p midpoint (Figure 1e), and posterior (Figure 1g) nasal septum regions developing at different rates. Measurements along the A-P (Figure 2A–C) axis demonstrated that the nasal bone (a,b in Figure 2B) and PPE (a–e in Figure2B) grew overall proportionally. This was evident by a linear correlation ($R^2 = 0.949$), although a biphasic growth was apparent (Figure 2D). The nasal bone length and PPE demonstrate an almost isometric relationship. Rapid growth was observed between PN0-PN14 and PN21-PN60. The period PN14-PN21 appeared more static. The same dynamic growth pattern was observed along the A-P axis for nasal cavity height (Figure 2E) and nasal septum length. Measurements at anterior, a–p midpoint, and posterior positions (Figure 2F, landmarks b,c and a–d, respectively, refer to Figure 1 for positions) revealed overall linear growth, although again a stalled period was apparent between PN14 and PN21. The increased posterior height when compared to anterior was reflected by the larger growth slope of 0.37 compared to 0.26. Up to PN14, growth rates among anterior, a–p midpoint, and posterior positions were quite similar but became more variable thereafter (Figure 2F). After PN14, the growth of the anterior nasal septum was reduced in comparison to the a–p midpoint and posterior nasal septum. The slopes of the anterior, a–p midpoint, and posterior nasal septum were 0.33, 0.38, and 0.38, respectively. Thus, the growth of the nasal septum is dynamic and undergoes growth spurts with stalled growth in between. Raw data obtained from the measurements demonstrated in Figure 2 are outlined in Table S1.

3.2 | Chondrocytes in the nasal septum undergo a position-dependent maturation process

To identify morphological changes that accompany nasal cartilage growth, we performed histological analysis at each developmental stage on anterior (Figure 3; Figure S1), a–p midpoint (Figure S1),

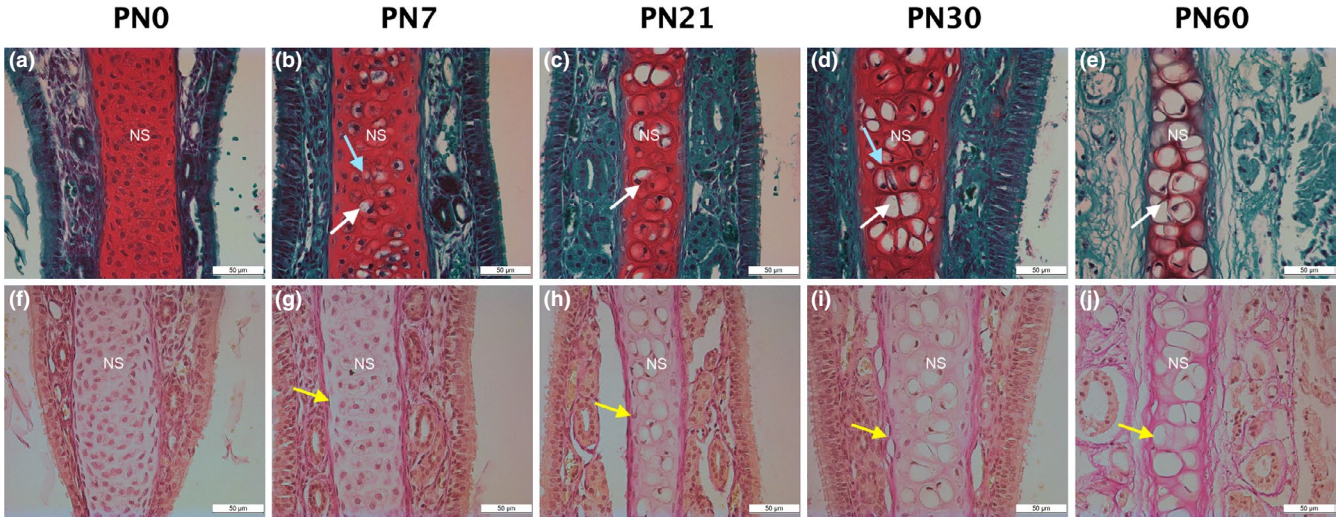

FIGURE 3 Chondrocytes in the anterior septum mature and develop a strong collagen network. Safranin O (a–e) and Van Gieson (f–j) staining of the anterior nasal septum on 7 μm paraffin sections. Hypertrophic-like chondrocytes become apparent after PN7 (white arrows). Collagen fibril formation (yellow arrow) starts in the perichondrium after PN7 to form a dense collagen network by PN60. Columnar-like chondrocytes were observed at PN7 and PN30 (blue arrows) NS, nasal septum

and posterior sections (Figure 4; Figure S1). The central portion of the nasal septum is shown for representative time-points only in Figures 3 and 4. For the full panel, refer to Figure S1. The most obvious change in the septal cartilage was the change in chondrocyte cell size and cellularity starting in the middle of septum. In general, the high number of small chondrocytes was replaced with time by fewer and much larger hypertrophic chondrocytes. In the anterior septum, the presence of hypertrophic-appearing chondrocytes was first noticed at PN7 (Figure 3b, white arrows). At PN60, the septum appeared to be entirely composed of large, hypertrophic chondrocytes (Figure 3a–e). Apart from this dynamic change in cell size, the width of the cartilage and perichondrium similarly changed. At the same time, the intensity of the Safranin O stain was reduced at PN60 indicative of a change in cartilage properties (Figure 3e). Lateral lining of collagen fibers along the presumptive perichondrium became first noticeable at PN7 and persisted through all subsequent stages (Figure 3f–j, yellow arrows). At PN60, but not at any earlier time-point, an extensive collagen network had formed anterior in between the large hypertrophic chondrocytes (Figure 3j). Results for Alcian Blue demonstrated similar morphological observations to those observed in sections stained with Safranin O (Figure S1). Results from the a–p midpoint nasal septum demonstrated similar morphological trends to those observed in the anterior nasal septum (Figure S2). Overall, it appeared that the chondrocytes in the anterior and a–p midpoint nasal septum undergo dynamic changes resulting in the formation of hypertrophic chondrocytes surrounded by a meshwork of dense collagen fibers.

In the posterior nasal septum, hypertrophic chondrocyte maturation (Figure 4, white arrows) started in the central portion of the septum and progressed more slowly. The large hypertrophic chondrocytes observed in the anterior/a–p midpoint septum were not seen (Figure 4e). The onset of collagen fibril formation (Figure 4h) coincided with the appearance of hypertrophic chondrocytes similar to the anterior septum. The increase in hypertrophic chondrocytes and collagen fiber formation appeared biphasic. The two stages with predominant hypertrophic chondrocytes at PN21 and PN60 were interrupted by the appearance of columnar chondrocytes reminiscent of the columns in the growth plate (Figure 4d, blue arrows). Columnar chondrocytes were more prevalent in the posterior septum. Similarly, collagen fiber formation followed a biphasic pattern. Dense collagen fibers were observed at PN21 and PN60 (Figure 4h,j, yellow arrows), but appeared reduced at PN30 (Figure 4i). Overall, assessing cartilage development on the basis of cartilage hypertrophy and collagen fiber formation revealed differences between the anterior and posterior septum and over time. Chondrocytes in the posterior nasal septum followed a biphasic pattern of hypertrophy. Anterior, a linear differentiation pattern was observed, and hypertrophic chondrocytes were eventually surrounded by a collagen mesh.

3.3 | Position-dependent differences in chondrocyte maturation are reflected in differences in ECM composition and cell differentiation

To correlate molecular changes to the morphological differences in the nasal septum, we stained for proteins commonly used to distinguish the various chondrocyte differentiation stages in the growth plate and articular cartilage (Gómez-Picos & Eames, 2015). Nuclear expression of Sox9 was only detected at E18.5 (Figure 5a,b), whereas expression at PN0 was more cytoplasmic (Figure 5c,d). Expression was stronger in anterior sections and no expression was observed at any of the later stages (Figure S3). Col II was ubiquitously expressed throughout the septum from E18.5 to P14, but subsequently steadily decreased showing only weak and more centrally located expression in the posterior

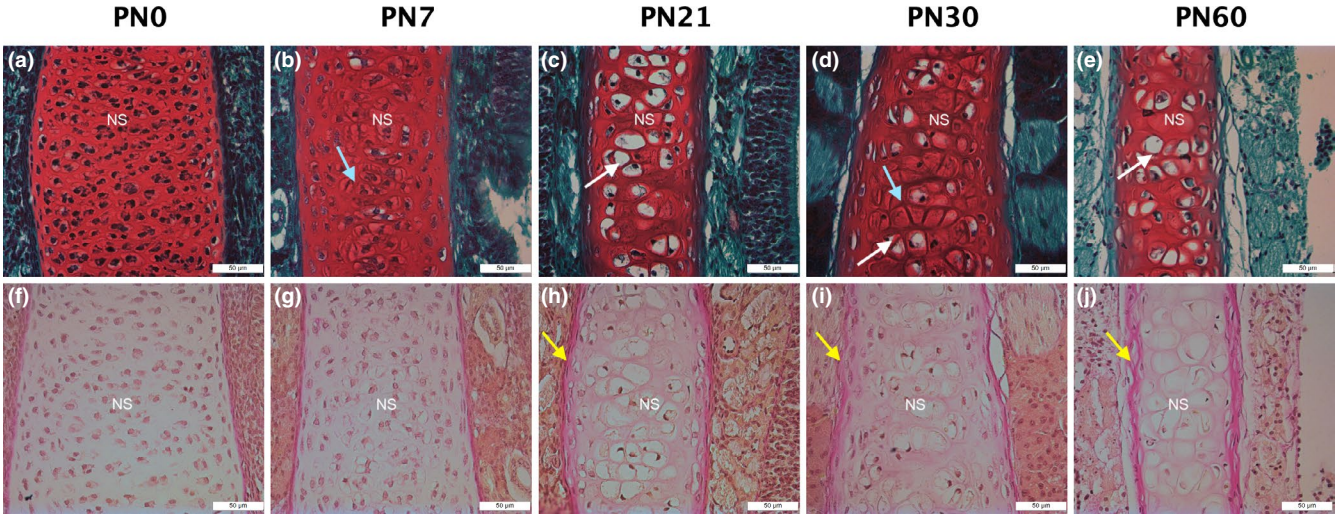

FIGURE 4 Chondrocytes in the posterior septum reflect biphasic growth. Safranin O (a–e) and Van Gieson (f–j) staining of the posterior nasal septum on 7 μm paraffin sections. Hypertrophic chondrocytes (c) prevalent from PN21 onwards (white arrows) and a reduction at PN30 reflect the biphasic growth. Columnar-like chondrocytes were observed at PN7 and PN30 (blue arrows). Collagen fibril formation is evident from PN21 (yellow arrow) onwards. Note: Absence of dense collagen network at PN60. NS, nasal septum

cartilage at PN60 (Figure 5i–l). Runx2 expression varied by location, time, and subcellular localization. At early stages (E18.5, PN0), expression was predominantly nuclear and more abundant posterior. Around PN7, expression was observed throughout the entire septum but was predominantly cytoplasmic (not shown). At PN30 expression was still abundant, but more restricted to the central part of the septum (Figure 6d). Col X was not observed before PN21 posterior and PN30 anterior and was predominantly observed in the lateral aspects of the septum (Figure 6g). At PN60, expression became stronger anterior compared to posterior (not shown). Mmp13 was detected first at PN0 in the posterior septum. The expression of Mmp13 appeared nuclear at most time-points. At PN14, its expression became more distinct and was mostly restricted to the center of the septum (Figure 6l). Expression persisted until PN60 in the posterior sections, albeit levels appeared reduced (not shown). Anterior, Mmp13 was observed only in the perichondrium (Figure 6i,k), although staining was difficult to distinguish from background (Figure S4). Sp7 was first detected in posterior regions at PN0. Expression was observed throughout the septum with both nuclear and cytoplasmic localization (Figure 7b). Expression almost disappeared by PN14 (Figure 7c,d). No or very limited expression was observed within septum cartilage anterior. At PN60, cytoplasmic expression could be observed in areas where the PPE would be expected. Anterior expression was cytoplasmic and restricted to the perichondrium. Ocn was already present at E18.5 (not shown).

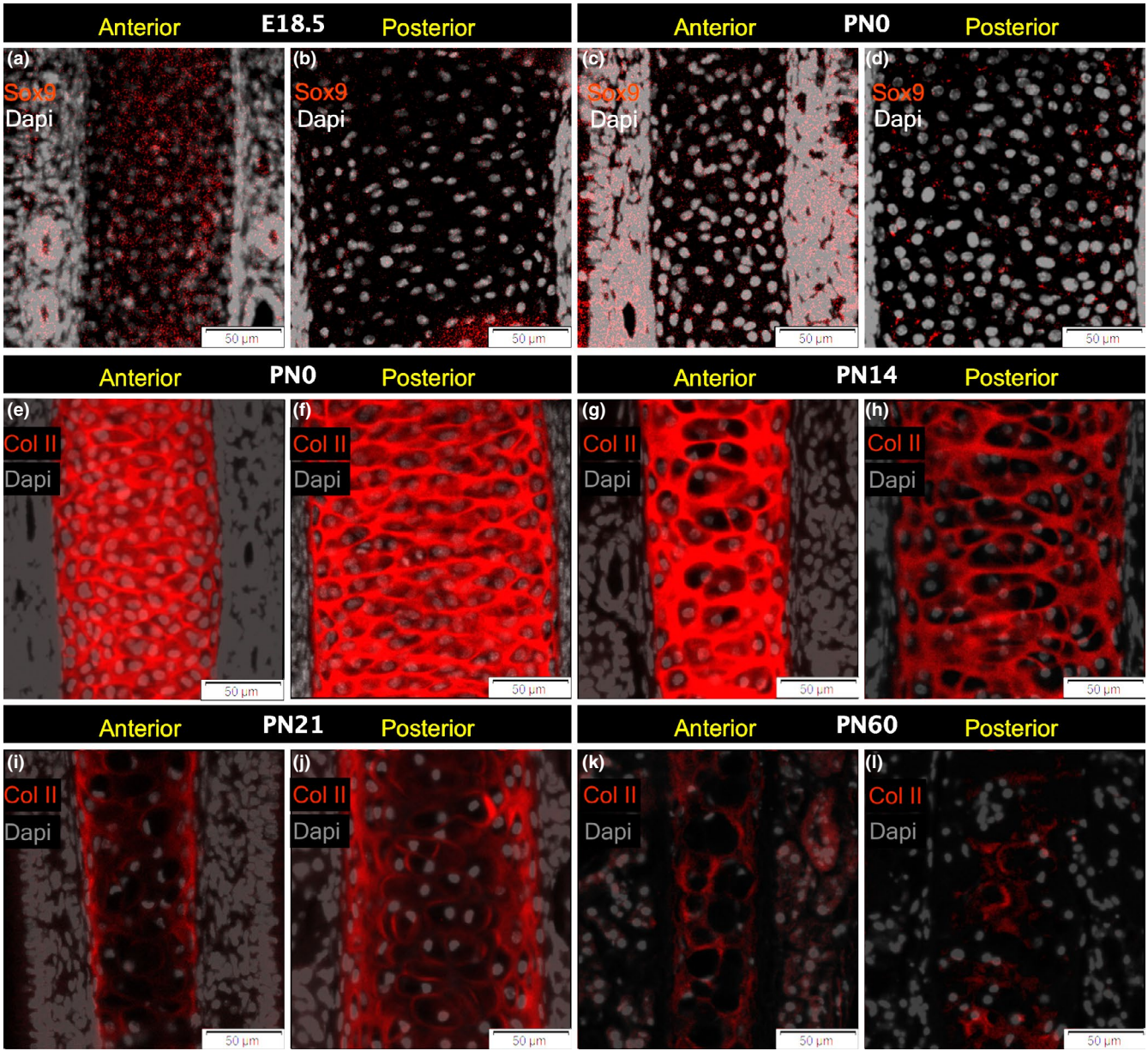

FIGURE 5 Proteins marking early chondrogenesis show anterior-posterior differences. Immunofluorescence staining for Sox9 (a–d) and Collagen II (Col II) (e–l) on 7 µm paraffin sections. Presence of Sox9 is only noted at E18 and PN0 and is more prominent in the anterior nasal septum. Presence of Col II decreases over time, which is more prominent in the posterior nasal septum at PN60 (l). (a,c,e,g,i,k) anterior sections, (b,d,f,h,j,l) posterior sections

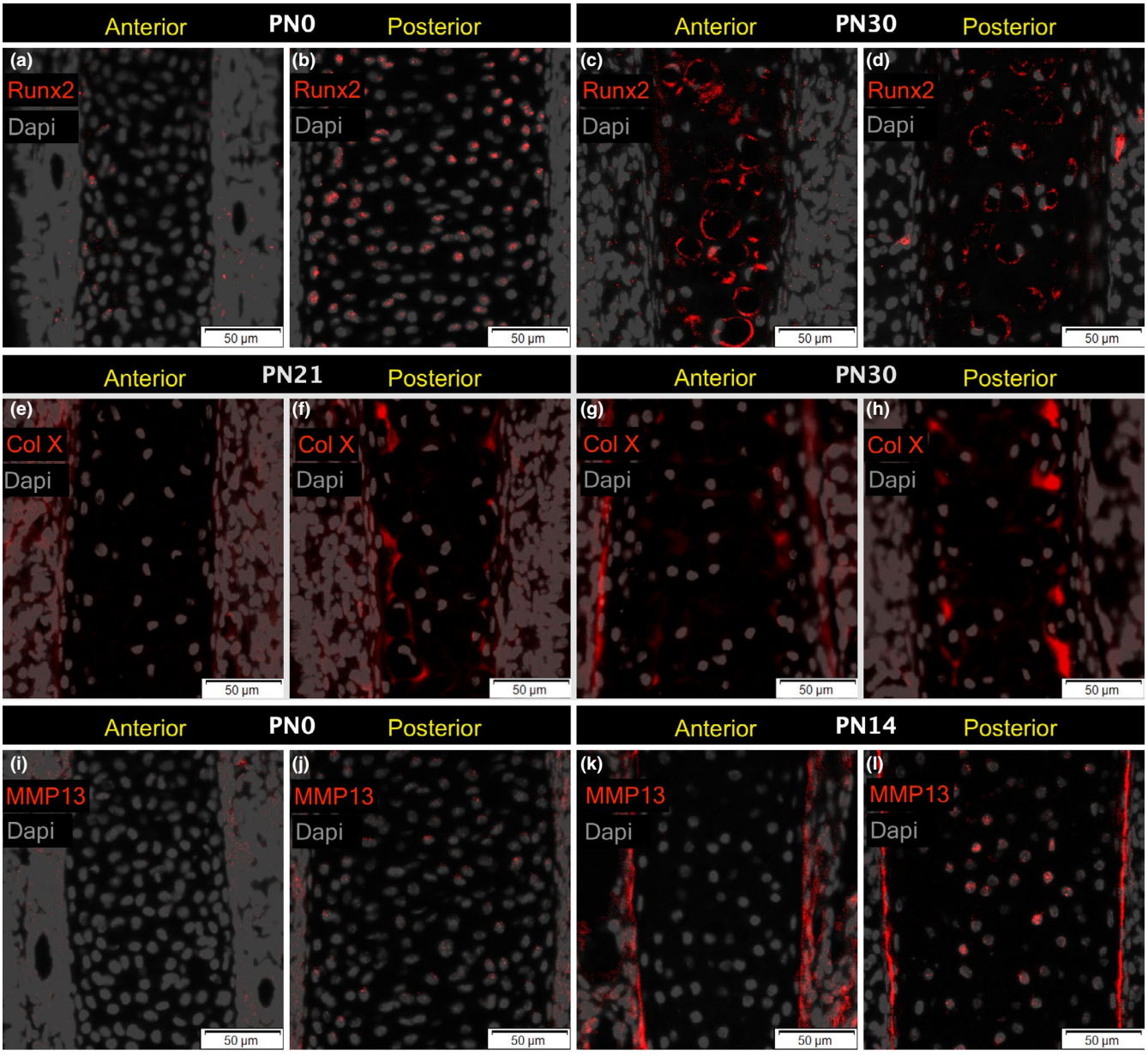

FIGURE 6 Proteins indicative of hypertrophic chondrocytes are dynamically expressed in anterior and posterior nasal septum. Immunofluorescence staining on anterior (a,c,e,g,i,k) and posterior (b,d,f,h,j,l) 7 µm paraffin sections at different ages. (a–d) Runx2 expression is initially nuclear (DAPI-grey) in both anterior and posterior septum and becomes ubiquitously cytoplasmic by PN30. (e–h) Collagen X (Col X) expression is evident posterior from P21 (f) onwards, whereas anterior Col X is not expressed until PN30 (g). (i–l) MMP13 is expressed at low levels posterior starting at PN0 (j) and becomes more apparent at PN14 (l). No expression of MMP13 is observed in the chondrocytes of the anterior nasal septum (i,k) at all ages except for PN7 (not shown)

Expression peaked at PN0 posterior and PN7 anterior (Figure 7g), and then steadily decreased to PN60 (Figure 7i). At PN60, anterior expression was predominately observed in the perichondrium but not posterior (Figure 7j).

3.4 | Spatiotemporal pattern of PPE ossification in the nasal septum

We next correlated the expression of hypertrophy (ColX, Mmp13) and ossification (Sp7, Ocn) markers with the spatiotemporal ossification of the PPE. PPE ossification was evident from PN7 onwards (Figure S5B) and the extent of ossification steadily increased through to PN60 (Figure S5F). Comparison of midsagittal slices from µCT scans of mice at PN30 and PN60 clearly indicated the increase in mineralization. PPE mineralization followed a superior to inferior trajectory (Figure 8a,g). Hypertrophic chondrocytes became successively incorporated into the bony matrix of the PPE (Figure 8b,d,h,j). Intensity of Safranin O staining decreased from PN30 to PN60 (Figure 8d,j) at sites of presumptive bone formation. A collagen matrix surrounded the PPE both at PN30 and PN60, but was more prominent at the older age (Figure 8c,i). Runx2 and Sp7 could both be observed at the sites of

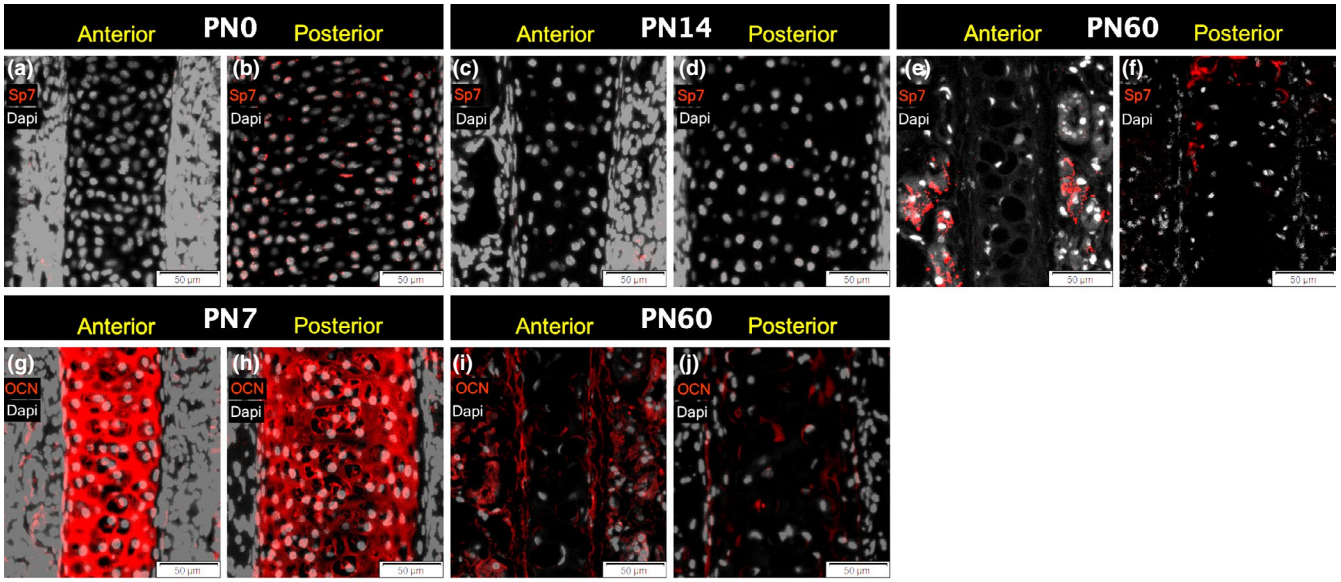

FIGURE 7 Bone-specific proteins are not restricted to the posterior region. Immunofluorescence staining on anterior (a,c,e,g,i) and posterior (b,d,f,h,j) 7 μm paraffin sections at different ages. (a–f) Sp7 is already restricted to the posterior nasal septum. It is first evident at PN0 (b), then expression is reduced (d) until the formation of bone in the posterior nasal septum at PN60 (f). Osteocalcin (Ocn) is highly expressed in chondrocytes from PN0 to PN7 (g–j) with stronger staining anterior. Expression becomes less over time both anterior and posterior

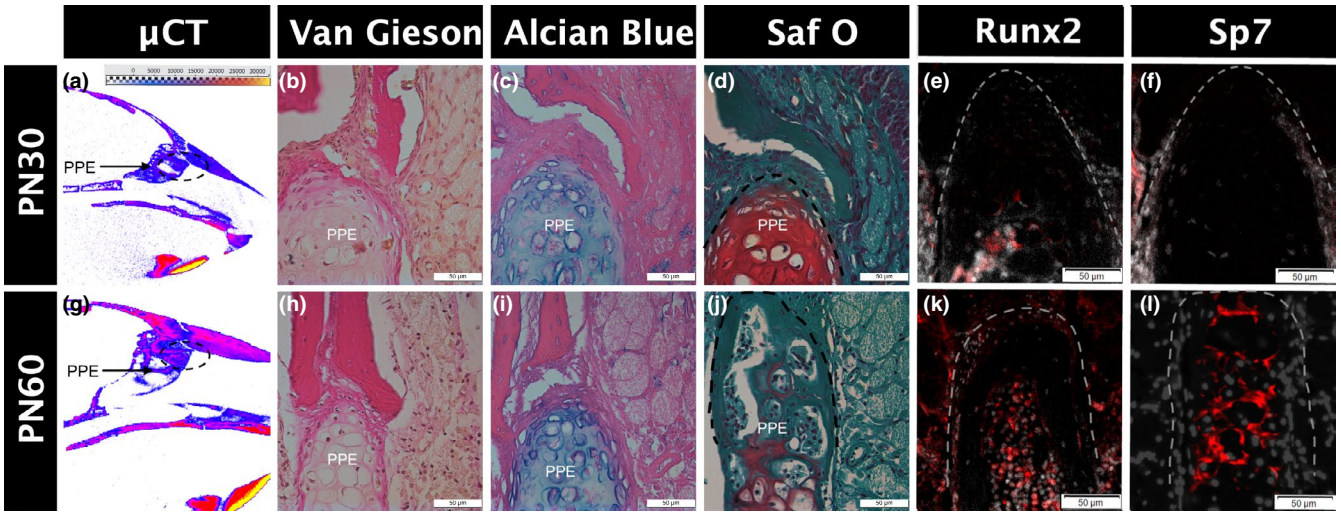

FIGURE 8 The perpendicular plate of the ethmoid (PPE) ossifies in a superior to inferior direction. (a,g) Midsagittal slice from micro-CT analysis shows highly calcified, mature (pink), and lesser calcified, immature bone at PN30 (a) and PN60 (g). Color map for false-colored mineral density is shown in a. Ossification (dotted oval) descends from dorsal (superior) to ventral (inferior). Van Gieson (b,h), Alcian Blue (c,i), and Safranin O (d,j) stains on posterior 7 μm paraffin sections at PN30 (b–d) and PN60 (h–j) indicate loss of Safranin O and increase in collagen fibers indicative of bone formation in PN60 nasal septum. Immunostaining for Runx2 (e,k) shows cytoplasmic staining at PN30 (e) and increased nuclear expression in the marrow space of the newly forming bone at PN60 (k). Sp7 (f,l) is restricted to PN60 (l) to sites of ossification

presumptive transformation of cartilage into bone. Whereas Runx2 was predominantly observed in hypertrophic chondrocytes still staining positive for Safranin O, the Sp7 expression domain was primarily associated with the ossified PPE. These findings suggest that nasal septum ossification follows a posterior-anterior and dorsal-ventral direction. Figure 9a provides a summary showing that protein expression varies over time and with location. Figure 9b demonstrates a proposed model for chondrocyte maturation and septum growth through hypertrophy, suggesting that nasal septum cartilage is a much more dynamic cartilaginous tissue than previously thought.

4 | DISCUSSION

In this study we correlated growth of the nasal cartilage with cellular properties across its length and over time. Although generally

defined as hyaline cartilage, we found that the nasal cartilage is a more complex and dynamic structure than anticipated that could only incompletely be described using commonly used markers for hyaline cartilage.

4.1 | Asynchronous growth phases in the nasal cavity over time

Previous studies (Vora et al., 2016; Wealthall & Herring, 2006) described the dynamic growth of the nasal complex in context of overall craniofacial growth. The nasal unit grows continuously and rapidly between PN7 and PN56, with individual aspects, such as nasal bone length or width, displaying different growth rates. Our data indicate that the nasal cartilage similarly grows heterogeneously. In particular, a reduced growth rate for the height of the nasal cartilage was observed between PN14 and PN21.

The growth pattern of the nasal septum has been deduced in the context of growth anomalies in children/adolescents such as midfacial hypoplasia and nasal septum deviation using a morphometric approach (Goergen et al., 2017) or in large animals mapping proliferation using a histological approach (Al Dayeh &

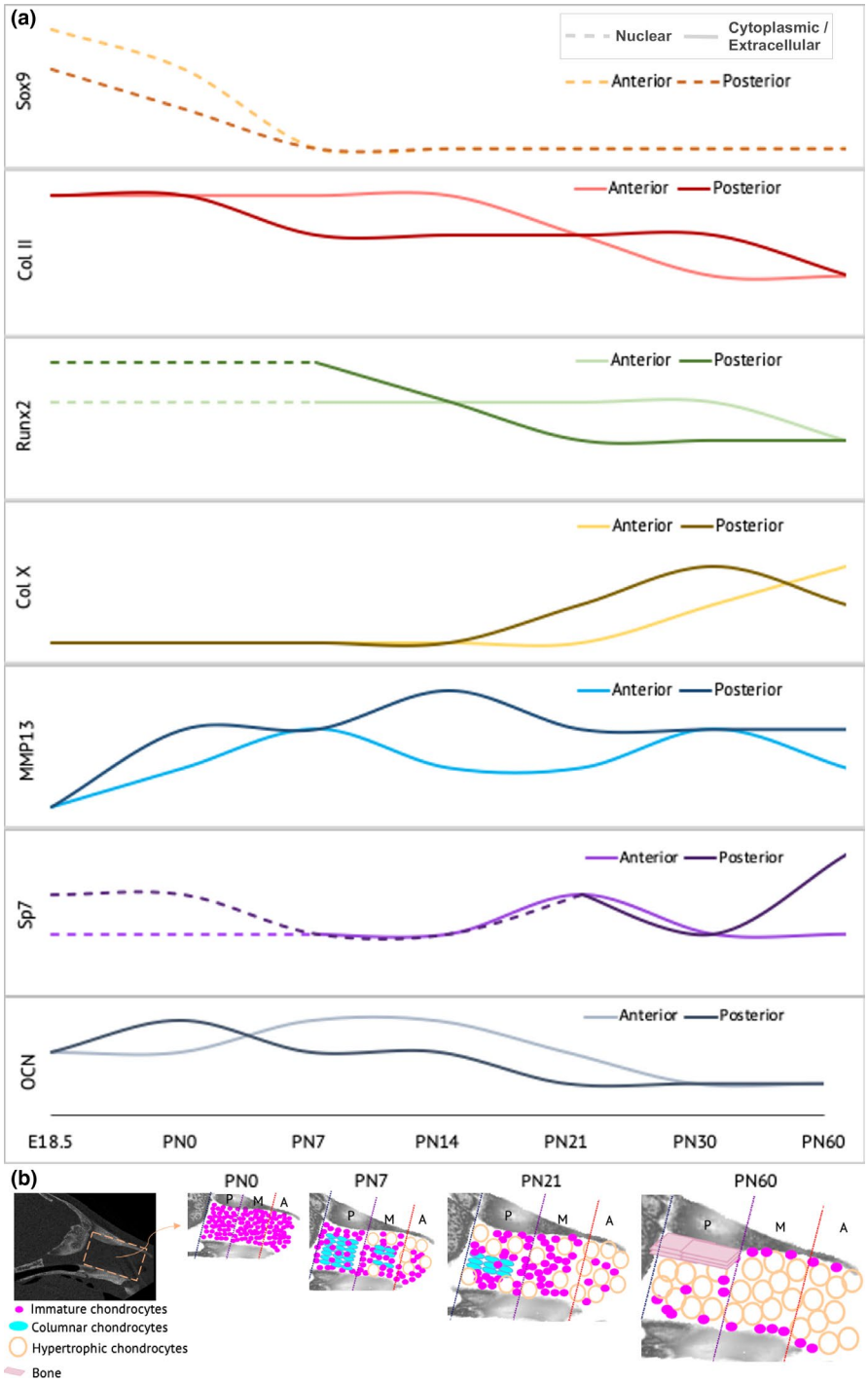

FIGURE 9 Illustration summarizing the dynamic expression of proteins involved in nasal cartilage development as well as the proposed model for nasal cartilage growth through hypertrophy. (a) Schematic is based on findings from all immunofluorescence experiments (n = 3/protein/age). Solid lines indicate cytoplasmic expression, dotted lines indicate nuclear expression. (b) Overlay on isosurface rendering of a μCT scan of an adult mouse indicating growth of immature chondrocytes, columnar chondrocytes, hypertrophic chondrocytes, and bone over time. Schematic is based on findings from all histological analysis (n = 3/age). Anterior (a) chondrocytes (red) mature first through the process of hypertrophy followed by a–p midpoint (M) (purple) and posterior (P) (blue) regions. μCT, micro-computed tomography

Herring, 2014; Al Dayeh et al., 2013; Gupta, 2011; Long et al., 1968). Measuring nasal septum growth at multiple positions along the A-P axis over time provides thus context for those studies. Growth and ossification of the PPE followed a posteroanterior and superior-inferior direction, in line with and extending previous results using Calcein tracing over a more restricted timeframe in PN0–PN15 mice (Wealthall & Herring, 2006). The cartilage followed the endochondral ossification pathway as previously suggested (Wealthall & Herring, 2006). Correlating mineralization at early and late stages with the expression of ossification markers suggest that a chondrocyte to osteoblast transdifferentiation process takes place at the PPE (Hu et al., 2017).

4.2 | Onset of chondrocyte hypertrophy coincides with appearance of collagen fiber network and growth of the nasal septum

Gross morphological analysis using Safranin O and Van Gieson staining demonstrated dynamic changes in cell size and density over time. Small immature chondrocytes were successively replaced by large hypertrophic chondrocytes. This change did not occur in a uniform fashion. These dynamic changes were accompanied by changes in septal cartilage width, which seemed to inversely correlate with the thickness of the perichondrium. In the anterior nasal septum, differentiation into hypertrophic chondrocytes started at PN7 (Figure 3b). Posterior, hypertrophic chondrocytes were not detected before PN21. Similarly, remodeling of the ECM coincided with chondrocyte maturation and differentiation. Based on these observations and the fact that no overt apoptosis can be observed (not shown), we propose that acquisition of hypertrophy and concomitant spatial redistribution of chondrocytes constitutes the major mechanism driving the three-dimensional growth of the septal cartilage (Figure 9b). Hypertrophy is first observed anterior, thus, this part of the septum matures first, followed by the appearance of a cartilage network surrounding each chondrocyte, while columnar stacks of chondrocytes are observed posterior and a–p midpoint. This is followed by hypertrophic maturation in the a–p midpoint and posterior regions. This form of growth driven by chondrocyte maturation is somewhat reminiscent to the developing synchondrosis in the cranial base, where chondrocyte growth ceases in an anteroposterior manner while ossification occurs in a posteroanterior direction (Hoyte, 1975). In the case of the nasal septal cartilage, differentiation toward posterior occurs last and only the posterior portion will ever ossify through the process of chondrocyte to osteoblast transdifferentiation. The anterior portion remains cartilaginous throughout. The early differentiation in the anterior region is in line with previously reported reduction in growth and proliferation (Yan et al., 2016). The appearance of an extensive collagen network surrounding the hypertrophic chondrocytes across the entire anterior region was noted, which could provide stiffness and increased mechanical resistance to the anterior nasal cartilage (Loparic et al., 2010). The stiffness of collagen fibrils has been shown to promote chondrocyte differentiation (Prein et al., 2016). Whether the formation of collagen fibrils triggers the early cell differentiation, or whether cell differentiation is a prerequisite for collagen network formation is not clear. In the posterior nasal septum, the onset of collagen fiber remodeling concurred with the appearance of hypertrophic chondrocytes, albeit at a later stage.

4.3 | Molecular properties contribute to ECM composition in the nasal septum

Studies on the growth zone of long bones have led to the identification of a set of molecular markers useful to follow hyaline cartilage differentiation (Chau et al., 2014). Using these markers, spatiotemporal changes in the nasal cartilage were mapped in an attempt to describe nasal hyaline cartilage differentiation/maturation. Expression of Sox9 and Col II largely followed the expected pattern. Sox9 was present in the early stages of nasal septum development at E18.5 and PN0 with expression subsiding at later stages. Coll II was ubiquitous throughout the septum with highest expression at early stages from PN0 to PN14, and only faint expression at PN60 remained in the posterior region. In the knee, Col II becomes diminished with age making it a less prominent ECM component of mature hyaline cartilage (Kozhemyakina et al., 2015). Runx2, a key regulator of bone formation, is expressed during most stages of cartilage maturation (Kozhemyakina et al., 2015). In progenitor cells, Runx2 promotes chondrocyte over adipocyte fate (Enomoto et al., 2004). Maybe not unexpected, widespread nuclear expression of Runx2 was observed at PN0, when chondrocytes were still immature. Whether this early expression is associated with a commitment to the chondrocyte lineage or serves some other, not yet recognized function is not clear. At later stages, Runx2 was more sparsely expressed and mostly observed in the cytoplasm. It has been shown that this shift from nuclear to cytoplasmic Runx2 localization is microtubule driven and has been associated with chondrocyte maturation in chick growth plate chondrocytes (Enomoto et al., 2004; Farquharson et al., 1999; Pockwinse et al., 2006). The role of cytoplasmic Runx2 in cartilage and bone is not understood. Nuclear Runx2 is seen in hypertrophic chondrocytes during endochondral ossification (Yang et al., 2017). Stronger cytoplasmic Runx2 expression was observed in the anterior nasal cartilage, which incidentally never ossifies compared to posterior where ossification occurs. The shift from cytoplasmic to nuclear Runx2 localization in the PPE coincided with ossification, whereas cytoplasmic localization correlated with an arrest in chondrocyte maturation.

Expression of Mmp13 is normally restricted to hypertrophic chondrocytes (Henriet & Eeckhout, 2013) and has been associated with collagen remodeling and degradation (Mitchell et al., 1996). In the posterior nasal septum, Mmp13 expression was already detected in immature chondrocytes from PN0 onwards. Expression was maintained until PN60, but expression decreased over time, in line with the association of reduced Mmp13 expression with hypertrophic chondrocyte proliferation in the growth plate (Henriet & Eeckhout, 2013). Whereas the role of Mmp13 at later stages of chondrocyte

development is well established, its role during early cartilage development is not well understood. In E15.5 Mmp13-deficient embryos, the growth plate was longer and columnar chondrocytes were misaligned (Inada et al., 2004), indicating a role in the spatial organization and growth of the developing cartilage. Growth plate length and organization of columnar chondrocytes are both dependent on collagen matrix remodeling (Prein et al., 2016). Mmp13 might play a similar role in the nasal cartilage.

Expression of Osterix/Sp7 differed from the expected expression pattern. Nuclear Sp7 was observed at PN0 in the posterior nasal septum, significantly earlier than the onset of posterior ossification. This early expression might reflect an early commitment to the bone lineage (Sepulveda et al., 2017). Ocn, a frequently used marker for osteoblast differentiation (Zoch et al., 2016), was expressed at all time-points both anterior and posterior. The strong expression in the anterior nasal septum suggests a role for Ocn other than ossification. The recent identification of an endocrine function for Ocn in the regulation of glucose metabolism (Wei & Karsenty, 2015) might indicate a similar function in cartilage.

Overall, the commonly used molecular markers to describe cartilage differentiation in the growth plate cannot be faithfully applied to the growing nasal septum. Whereas presence of Sox9, Runx2, and Sp7 in the growing nasal cartilage is in line with the gene regulatory networks described for immature cartilage, mature cartilage, and bone based on the fossil record (Gómez-Picos & Eames, 2015), Safranin O and Alcian Blue clearly ascertain chondrocyte properties to these cells. Additional signaling networks must contribute to the subspecification of chondrocytes.

4.4 | Differences between nasal septum and growth plate cartilage

The nasal septum cartilage and growth plate cartilage are both hyaline cartilages albeit with different functional requirements. The growth plate is physically organized into subzones such as resting, proliferating, hypertrophic, and ossification zone. The clear distinction of these subzones is not observed in the nasal septum (Hallett et al., 2019). Growth plate properties are present at the septoethmoidal junction at least till P15, although later time-points were not analyzed (Wealthall & Herring, 2006). The same study also proposed that some septum growth must occur by interstitial cartilage expansion. Here, we show that the mechanism for this appears to be chondrocyte hypertrophy. The growth plate contributes primarily to the longitudinal growth of the limb, whereas the nasal septum needs to grow in all dimensions. In the growth plate, organized stacks of columnar chondrocytes are observed allowing for synchronous coordinated growth (Hall & Miyake, 2000; Yan et al., 2016). In the septum, columnar stacks are present, but their stacking is horizontal and appears asynchronous. This interspersed stacking may contribute to the observed heterogeneous growth. Whereas the columnar chondrocytes in the growth plate contribute to the elongation of the bone (Kobayashi et al., 2005), the horizontal stacking in the nose would be expected to contribute to nasal septum width. Indeed, rod-shaped cartilages like the nasal septum have transverse clonal arrangements that contribute to the diameter of the cartilaginous rod (Kaucka et al., 2017). The interspersed clonal arrangements could be a reflection of asynchronous differentiation of the cartilage itself. The transverse columns were centrally located and hypertrophic chondrocytes were interspersed between them (Claassen et al., 2017). In the growth zone, the longitudinal stacking of columnar chondrocytes is regulated by Parathyroid hormone-related protein and Indian Hedgehog (Mizuhashi et al., 2018). Whether the same signaling networks are also active in the nasal septum is yet to be investigated.

The majority of the nasal septum does not ossify, with the exception of the posterior region. During endochondral ossification, hypertrophic chondrocytes either undergo apoptosis to allow for invasion of osteoprogenitors and vasculature (Gibson, 1998; Ortega et al., 2004), or directly transdifferentiate into osteoblasts (Aghajanian & Mohan, 2018). It has been speculated that the fate of hypertrophic chondrocytes during endochondral ossification might depend on the type of hyaline cartilage, its stage of development, and the cellular location within (Aghajanian & Mohan, 2018; Cervantes-Diaz et al., 2017; Gibson, 1998; Gómez-Picos & Eames, 2015; Ortega et al., 2004). In the PPE, expression of Runx2 and SP7 in relation to histological stains suggests that transdifferentiation might be the prominent mechanism (Zhou et al., 2014). However, formal proof using detailed lineage tracing would be required to ascertain this.

Our study adds to previous literature on nasal septum cartilage. It shows that cartilage differentiation in the nasal septum does not follow a homogenous differentiation path as set out in growth plate cartilage. The observed spatiotemporal variation was unexpected. Whereas the posterior septum appeared to follow the path of endochondral ossification, the anterior septum develops properties atypical for hyaline cartilage, such as extensive collagen networks. It will be of interest to see if and which of those cartilage properties are altered in a deviated septum or a septum with stunted growth. This study also highlights the need to carefully investigate different hyaline cartilages to better understand their functional specialization. Lastly, the current perception of the nasal cartilage as a hyaline cartilage akin to articular cartilage is quite likely an oversimplification. The dynamic molecular and cellular heterogeneity observed along the length of the septum will need to be considered when using this cartilage for tissue engineering.

ACKNOWLEDGMENTS

This work was supported by Natural Science and Engineering Research Council of Canada RGPIN-2014-06311 and funds from the School of Dentistry, University of Alberta (all to DG). The authors would like to thank Brian F Eames for critical reading of the manuscript.

CONFLICT OF INTEREST

The author(s) declare no conflict of interest.

AUTHOR CONTRIBUTIONS

PB: concept/design, acquisition of data, data analysis/interpretation, drafting of manuscript, critical revision of the manuscript, and approval of the article. TK: acquisition of data, data analysis/interpretation, drafting of manuscript, critical revision of the manuscript,and approval of the article. AA: analyzed data, critical revision of the manuscript, and approval of the article. DG: concept/design, data interpretation, drafting, critical revision of manuscript, and approval of the article.

DATA AVAILABILITY STATEMENT

The data that support the findings of this study are available from the corresponding author upon reasonable request.

ORCID

Pranidhi Baddam https://orcid.org/0000-0003-0232-2022
Tiffany Kung https://orcid.org/0000-0002-9406-5934
Adetola B. Adesida https://orcid.org/0000-0003-1798-6251
Daniel Graf https://orcid.org/0000-0003-1163-8117

REFERENCES

Aghajanian, P. & Mohan, S. (2018) The art of building bone: emerging role of chondrocyte-to-osteoblast transdifferentiation in endochondral ossification. *Bone Research*, 6, 19. https://doi.org/10.1038/s41413-018-0021-z

Al Dayeh, A.A. & Herring, S.W. (2014) Cellular proliferation in the nasal septal cartilage of juvenile minipigs. *Journal of Anatomy*, 225, 604–613. https://doi.org/10.1111/joa.12237

Al Dayeh, A.A., Rafferty, K.L., Egbert, M. & Herring, S.W. (2013) Real-time monitoring of the growth of the nasal septal cartilage and the nasofrontal suture. *American Journal of Orthodontics and Dentofacial Orthopedics*, 143, 773–783. https://doi.org/10.1016/j.ajodo.2013.01.012

Bi, W., Deng, J.M., Zhang, Z., Behringer, R.R. & de Crombrugghe, B. (1999) Sox9 is required for cartilage formation. *Nature Genetics*, 22, 85–89. https://doi.org/10.1038/8792

Cattell, M., Lai, S., Cerny, R. & Medeiros, D.M. (2011) A new mechanistic scenario for the origin and evolution of vertebrate cartilage. *PLoS One*, 6, e22474. https://doi.org/10.1371/journal.pone.0022474

Cervantes-Diaz, F., Contreras, P. & Marcellini, S. (2017) Evolutionary origin of endochondral ossification: the transdifferentiation hypothesis. *Development Genes and Evolution*, 227, 121–127. https://doi.org/10.1007/s00427-016-0567-y

Chau, M., Lui, J.C., Landman, E.B.M., Späth, S.-S., Vortkamp, A., Baron, J. et al. (2014) Gene expression profiling reveals similarities between the spatial architectures of postnatal articular and growth plate cartilage. *PLoS One*, 9, e103061. https://doi.org/10.1371/journal.pone.0103061

Claassen, H., Schicht, M., Fleiner, B., Hillmann, R., Hoogeboom, S., Tillmann, B. et al. (2017) Different patterns of cartilage mineralization analyzed by comparison of human, porcine, and bovine laryngeal cartilages. *Journal of Histochemistry and Cytochemistry*, 65, 367–379. https://doi.org/10.1369/0022155417703025

D'Ascanio, L., Lancione, C., Pompa, G., Rebuffini, E., Mansi, N. & Manzini, M. (2010) Craniofacial growth in children with nasal septum deviation: a cephalometric comparative study. *International Journal of Pediatric Otorhinolaryngology*, 74, 1180–1183. https://doi.org/10.1016/j.ijporl.2010.07.010

Enomoto, H., Furuichi, T., Zanma, A., Yamana, K., Yoshida, C., Sumitani, S. et al. (2004) Runx2 deficiency in chondrocytes causes adipogenic changes in vitro. *Journal of Cell Science*, 117, 417–425. https://doi.org/10.1242/jcs.00866

Farquharson, C., Lester, D., Seawright, E., Jefferies, D. & Houston, B. (1999) Microtubules are potential regulators of growth-plate chondrocyte differentiation and hypertrophy. *Bone*, 25, 405–412. https://doi.org/10.1016/s8756-3282(99)00187-8

Gibson, G. (1998) Active role of chondrocyte apoptosis in endochondral ossification. *Microscopy Research and Technique*, 43, 191–204. https://doi.org/10.1002/(SICI)1097-0029(19981015)43:2<191:AID-JEMT10>3.0.CO;2-T

Goergen, M.J., Holton, N.E. & Grünheid, T. (2017) Morphological interaction between the nasal septum and nasofacial skeleton during human ontogeny. *Journal of Anatomy*, 230, 689–700. https://doi.org/10.1111/joa.12596

Gómez-Picos, P. & Eames, B.F. (2015) On the evolutionary relationship between chondrocytes and osteoblasts. *Frontiers in Genetics*, 6, 297. https://doi.org/10.3389/fgene.2015.00297

Grogan, S.P., Miyaki, S., Asahara, H., D'Lima, D.D. & Lotz, M.K. (2009) Mesenchymal progenitor cell markers in human articular cartilage: normal distribution and changes in osteoarthritis. *Arthritis Research & Therapy*, 11, R85. https://doi.org/10.1186/ar2719

Gupta, R.C. (2011) *Reproductive and developmental toxicology*. Elsevier. https://doi.org/10.1016/C2009-0-62417-X

Hall, B.K. & Miyake, T. (2000) All for one and one for all: condensations and the initiation of skeletal development. *BioEssays*, 22, 138–147. https://doi.org/10.1002/(SICI)1521-1878(200002)22:2<138:AID-BIES5>3.0.CO;2-4

Hall, B.K. & Precious, D.S. (2013) Cleft lip, nose, and palate: the nasal septum as the pacemaker for midfacial growth. *Oral Surgery, Oral Medicine, Oral Pathology and Oral Radiology*, 115, 442–447. https://doi.org/10.1016/j.oooo.2012.05.005

Hallett, S.A., Ono, W. & Ono, N. (2019) Growth plate chondrocytes: skeletal development, growth and beyond. *International Journal of Molecular Sciences*, 20, 6009. https://doi.org/10.3390/ijms20236009

Harkema, J. (2015) *Comparative anatomy and epithelial cell biology of the nose. Comparative biology of the normal lung*, 2nd edition. https://doi.org/10.1016/B978-0-12-404577-4.00002-3

Henriet, P. & Eeckhout, Y. (2013) Chapter 154—matrix metallopeptidase-13/collagenase 3. In: Rawlings, N.D. & Salvesen, G. (Eds.) *Handbook of proteolytic enzymes*, 3rd edition. Academic Press, pp. 734–744. https://doi.org/10.1016/B978-0-12-382219-2.00154-X

Hojo, H., Ohba, S., He, X., Lai, L.P. & McMahon, A.P. (2016) Sp7/Osterix is restricted to bone-forming vertebrates where it acts as a Dlx co-factor in osteoblast specification. *Developmental Cell*, 37, 238–253. https://doi.org/10.1016/j.devcel.2016.04.002

Hoyte, D.A. (1975) A critical analysis of the growth in length of the cranial base. *Birth Defects Original Article Series*, 11, 255–282.

Hu, D.P., Ferro, F., Yang, F., Taylor, A.J., Chang, W., Miclau, T. et al. (2017) Cartilage to bone transformation during fracture healing is coordinated by the invading vasculature and induction of the core pluripotency genes. *Development*, 144, 221–234. https://doi.org/10.1242/dev.130807

IHC WORLD. Protocol database—histology, immunohistochemistry, molecular and cell biology [WWW Document]. n.d. Available at: http://www.ihcworld.com/protocol_database.htm [Accessed 6th May 2020].

Inada, M., Wang, Y., Byrne, M.H., Rahman, M.U., Miyaura, C., López-Otín, C. et al. (2004) Critical roles for collagenase-3 (Mmp13) in development of growth plate cartilage and in endochondral ossification. *Proceedings of the National Academy of Sciences of the United States of America*, 101, 17192–17197. https://doi.org/10.1073/pnas.0407788101

Kaucka, M., Zikmund, T., Tesarova, M., Gyllborg, D., Hellander, A., Jaros, J. et al. (2017) Oriented clonal cell dynamics enables accurate growth

and shaping of vertebrate cartilage. *eLife*, 6. https://doi.org/10.7554/eLife.25902

Kemble, J.V. (1973) The importance of the nasal septum in facial development. *Journal of Laryngology and Otology*, 87, 379–386. https://doi.org/10.1017/s0022215100077021

Kim, I.-S., Lee, M.-Y., Lee, K.-I., Kim, H.-Y. & Chung, Y.-J. (2008) Analysis of the development of the nasal septum according to age and gender using MRI. *Clinical and Experimental Otorhinolaryngology*, 1, 29–34. https://doi.org/10.3342/ceo.2008.1.1.29

Kobayashi, T., Soegiarto, D.W., Yang, Y., Lanske, B., Schipani, E., McMahon, A.P. et al. (2005) Indian hedgehog stimulates periarticular chondrocyte differentiation to regulate growth plate length independently of PTHrP. *Journal of Clinical Investigation*, 115, 1734–1742. https://doi.org/10.1172/JCI24397

Kozhemyakina, E., Lassar, A.B. & Zelzer, E. (2015) A pathway to bone: signaling molecules and transcription factors involved in chondrocyte development and maturation. *Development*, 142, 817–831. https://doi.org/10.1242/dev.105536

Las Heras, F., Gahunia, H.K. & Pritzker, K.P.H. (2012) Articular cartilage development: a molecular perspective. *Orthopedic Clinics of North America*, 43(2), 155–171. https://doi.org/10.1016/j.ocl.2012.01.003

Long, R., Greulich, R.C. & Sarnat, B.G. (1968) Regional variations in chondrocyte proliferation in the cartilaginous nasal septum of the growing rabbit. *Journal of Dental Research*, 47, 505. https://doi.org/10.1177/00220345680470033601

Loparic, M., Wirz, D., Daniels, A.U., Raiteri, R., Vanlandingham, M.R., Guex, G. et al. (2010) Micro- and nanomechanical analysis of articular cartilage by indentation-type atomic force microscopy: validation with a gel-microfiber composite. *Biophysical Journal*, 98, 2731–2740. https://doi.org/10.1016/j.bpj.2010.02.013

Marconi, A., Hancock-Ronemus, A. & Gillis, J.A. (2020) Adult chondrogenesis and spontaneous cartilage repair in the skate, *Leucoraja erinacea*. *eLife*, 9, e53414. https://doi.org/10.7554/eLife.53414

Mitchell, P.G., Magna, H.A., Reeves, L.M., Lopresti-Morrow, L.L., Yocum, S.A., Rosner, P.J. et al. (1996) Cloning, expression, and type II collagenolytic activity of matrix metalloproteinase-13 from human osteoarthritic cartilage. *Journal of Clinical Investigation*, 97, 761–768. https://doi.org/10.1172/JCI118475

Mizuhashi, K., Ono, W., Matsushita, Y., Sakagami, N., Takahashi, A., Saunders, T.L. et al. (2018) Resting zone of the growth plate houses a unique class of skeletal stem cells. *Nature*, 563, 254–258. https://doi.org/10.1038/s41586-018-0662-5

Moss, M.L., Bromberg, B.E., Song, I.C. & Eisenman, G. (1968) The passive role of nasal septal cartilage in mid-facial growth. *Plastic and Reconstructive Surgery*, 41, 536–542. https://doi.org/10.1097/00006534-196806000-00004

Mumme, M., Barbero, A., Miot, S., Wixmerten, A., Feliciano, S., Wolf, F. et al. (2016) Nasal chondrocyte-based engineered autologous cartilage tissue for repair of articular cartilage defects: an observational first-in-human trial. *Lancet*, 388, 1985–1994. https://doi.org/10.1016/S0140-6736(16)31658-0

Ortega, N., Behonick, D.J. & Werb, Z. (2004) Matrix remodeling during endochondral ossification. *Trends in Cell Biology*, 14, 86–93. https://doi.org/10.1016/j.tcb.2003.12.003

Pockwinse, S.M., Rajgopal, A., Young, D.W., Mujeeb, K.A., Nickerson, J., Javed, A. et al. (2006) Microtubule-dependent nuclear-cytoplasmic shuttling of Runx2. *Journal of Cellular Physiology*, 206, 354–362. https://doi.org/10.1002/jcp.20469

Prein, C., Warmbold, N., Farkas, Z., Schieker, M., Aszodi, A. & Clausen-Schaumann, H. (2016) Structural and mechanical properties of the proliferative zone of the developing murine growth plate cartilage assessed by atomic force microscopy. *Matrix Biology*, 50, 1–15. https://doi.org/10.1016/j.matbio.2015.10.001

Robins, S.P., Seibel, M.J. & Bilezikian, J.P. (2006) *Dynamics of bone and cartilage metabolism*, 2nd edition. Elsevier. https://doi.org/10.1016/B978-0-12-088562-6.X5000-6

Sarnat, B.G. & Wexler, M.R. (1967) The snout after resection of nasal septum in adult rabbits. *Archives of Otolaryngology*, 86, 463–466. https://doi.org/10.1001/archotol.1967.00760050465021

Sepulveda, H., Aguilar, R., Prieto, C.P., Bustos, F., Aedo, S., Lattus, J. et al. (2017) Epigenetic signatures at the RUNX2-P1 and Sp7 gene promoters control osteogenic lineage commitment of umbilical cord-derived mesenchymal stem cells. *Journal of Cellular Physiology*, 232, 2519–2527. https://doi.org/10.1002/jcp.25627

Stenström, S.J. & Thilander, B.L. (1970) Effects of nasal septal cartilage resections on young guinea pigs. *Plastic and Reconstructive Surgery*, 45, 160–170. https://doi.org/10.1097/00006534-197002000-00010

Varela-Eirin, M., Loureiro, J., Fonseca, E., Corrochano, S., Caeiro, J.R., Collado, M. et al. (2018) Cartilage regeneration and ageing: targeting cellular plasticity in osteoarthritis. *Ageing Research Reviews*, 42, 56–71. https://doi.org/10.1016/j.arr.2017.12.006

Vora, S.R., Camci, E.D. & Cox, T.C. (2016) Postnatal ontogeny of the cranial base and craniofacial skeleton in male C57BL/6J mice: a reference standard for quantitative analysis. *Frontiers in Physiology*, 6, 417. https://doi.org/10.3389/fphys.2015.00417

Wealthall, R.J. & Herring, S.W. (2006) Endochondral ossification of the mouse nasal septum. *The Anatomical Record. Part A, Discoveries in Molecular, Cellular, and Evolutionary Biology*, 288, 1163–1172. https://doi.org/10.1002/ar.a.20385

Wei, J. & Karsenty, G. (2015) An overview of the metabolic functions of osteocalcin. *Current Osteoporosis Reports*, 13, 180–185. https://doi.org/10.1007/s11914-015-0267-y

Westreich, R.W., Burstein, D. & Fraser, M. (2011) The effect of facial asymmetry on nasal deviation. *Facial Plastic Surgery*, 27, 397–412. https://doi.org/10.1055/s-0031-1288923

Yan, B., Zhang, Z., Jin, D., Cai, C., Jia, C., Liu, W. et al. (2016) mTORC1 regulates PTHrP to coordinate chondrocyte growth, proliferation and differentiation. *Nature Communications*, 7, 11151. https://doi.org/10.1038/ncomms11151

Yang, M., Arai, A., Udagawa, N., Hiraga, T., Lijuan, Z., Ito, S. et al. (2017) Osteogenic factor Runx2 marks a subset of leptin receptor-positive cells that sit atop the bone marrow stromal cell hierarchy. *Scientific Reports*, 7, 4928. https://doi.org/10.1038/s41598-017-05401-1

Zhou, X., von der Mark, K., Henry, S., Norton, W., Adams, H. & de Crombrugghe, B. (2014) Chondrocytes transdifferentiate into osteoblasts in endochondral bone during development, postnatal growth and fracture healing in mice. *PLoS Genetics*, 10, e1004820. https://doi.org/10.1371/journal.pgen.1004820

Zoch, M.L., Clemens, T.L. & Riddle, R.C. (2016) New insights into the biology of osteocalcin. *Bone*, 82, 42–49. https://doi.org/10.1016/j.bone.2015.05.046

SUPPORTING INFORMATION

Additional supporting information may be found online in the Supporting Information section.

How to cite this article: Baddam P, Kung T, Adesida AB, Graf D, et al. Histological and molecular characterization of the growing nasal septum in mice. *J. Anat*. 2021;238:751–764. https://doi.org/10.1111/joa.13332